

THE DESIGN AND TESTING OF A WINGLET AIRFOIL FOR LOW-SPEED AIRCRAFT

Mark D. Maughmer^{*}, Timothy S. Swan[†], and Steven M. Willits[‡]
The Pennsylvania State University
University Park, Pennsylvania 16802

Abstract

The PSU 94-097 airfoil has been designed for use on winglets of high-performance sailplanes. The design problem is difficult because the airfoil must operate over a wide range of Reynolds numbers, and this range includes values that are relatively low. To validate the design tools, as well as the design itself, the airfoil was tested in the Penn State Low-Speed, Low-Turbulence Wind Tunnel from Reynolds numbers of 2.4×10^5 to 1.0×10^6 . In addition to free-transition measurements, potential drag reductions using artificial turbulators were explored, although the benefits were found to be limited for this application. Finally, performance predictions from two well-known computer codes are compared to the data obtained experimentally, and both are found to generate results that are in good agreement with the wind-tunnel measurements.

Nomenclature

c	airfoil chord
c_d	profile-drag coefficient
c_l	section lift coefficient
c_m	section pitching-moment coefficient about the quarter-chord point
C_p	pressure coefficient, $(p_l - p_\infty)/q_\infty$
p	static pressure, Pa (lb_f/ft^2)
q	dynamic pressure, Pa (lb_f/ft^2)
R	Reynolds number based on free-stream conditions and airfoil chord
x	airfoil abscissa
y	airfoil ordinate
α	angle of attack relative to x-axis, deg

Subscripts

l	local point on airfoil
max	maximum
W	wing
WL	winglet
∞	free-stream conditions

Introduction

The on-going process to improve the performance of modern sailplanes has resulted in vehicles having a level of aerodynamic refinement that is quite remarkable. Competition sailplanes in classes that are restricted to maximum allowable wingspans of fifteen meters have achieved lift-to-drag ratios of nearly 50:1, while gliders in the class without a span restriction have spans of over thirty meters, aspect ratios over fifty, and maximum lift-to-drag ratios in excess of 65:1.

The design of a successful high-performance sailplane is, however, significantly more difficult than striving only to maximize the lift-to-drag ratio. This is because in flying cross-country, the sailplane must be able to climb effectively in thermals, as well as be able to glide efficiently between thermals at high speeds. Thus, a successful design must balance the conflicting requirements of climbing and cruising over a broad range of possible soaring conditions.¹ To climb efficiently, a sailplane must be able to circle tightly with a low sink rate at low speeds and high lift coefficients. For these flight conditions, the induced drag is the largest contribution to the total drag. Inter-thermal cruise, on the other hand, corresponds to flight at high speeds and low lift coefficients, and the profile drag is the largest contributor.

To further improve the performance of sailplanes, efforts have been on going since the late 1980's to design winglets specifically for this application,² the design goal being to reduce the induced drag more than the additional area increases the profile drag. Because the induced drag decreases and the profile drag increases with increasing airspeed, the outcome of this trade-off is strongly dependent on airspeed. Thus, the gains in performance that winglets provide are greatest at low speeds and progressively less as the airspeed increases. For these reasons, the airfoil used on the winglets is a critical factor in whether or not the winglets operate as desired. To benefit the low-speed climb, the airfoil must achieve a reasonably high

Presented as Paper 2001-2478 at the AIAA 19th Applied Aerodynamics Conference, Anaheim, CA, June 11-14 2001. Copyright ©2001 by Mark D. Maughmer. Published by the American Institute of Aeronautics and Astronautics, Inc., with permission

^{*}Professor, Department of Aerospace Engineering, Senior Member AIAA.

[†]Graduate Assistant, Department of Aerospace Engineering, Member AIAA.

[‡]Research Engineer, Applied Research Laboratory, Member AIAA.

maximum lift coefficient, while at high speeds and low lift coefficients, low profile drag is crucial. To satisfy these requirements, an airfoil has been specifically designed for this application.

Design Requirements

Because a winglet does not operate exactly as a wing does, the performance benefits if the airfoil used is designed specifically for that purpose. To do this, it is necessary to fully determine the operational conditions of the winglet and how they relate to those of the wing. Because the principal benefit of a winglet is in climb, the airfoil performance at low flight speeds is of primary importance. Thus, the airfoil must generate the maximum lift coefficient required by the winglet as the aircraft main wing approaches stall. Likewise, low-drag performance over the entire operating range is important, but must be considered in conjunction with other constraints. As the profile drag increases with velocity squared, a large drag coefficient at low lift coefficients would severely penalize the aircraft performance at higher flight speeds. This drives the low lift-coefficient portion of the airfoil drag polar. The degree to which these considerations influence the overall performance is difficult to ascertain without considering the entire flight profile of the sailplane. To do this, a method of sailplane performance has been developed that can be used to determine how much of a gain at low speed is needed to offset a loss at high speed.³

As in most airfoil design efforts, the goal of the winglet airfoil design is to generate the lift required with the lowest possible drag. To determine the relationship between the lift-coefficient operating range of the winglet relative to that of the wing, a preliminary design effort was undertaken using an analysis method that is applicable to non-planar wings.³ The result of this effort, presented in Fig. 1, is the operational lift coefficients for the winglet as they depend on those of the wing. The flow field induced on the winglet by the wing is such that the range of lift coefficients over which the winglet operates is narrower than that of the wing. For the best performance, the operational low-drag range of the winglet airfoil should correspond to that of the main wing. As shown in Fig. 1, while the wing airfoil has a low-drag range from lift coefficients of 0.3 to just over 1.0, the corresponding range for the winglet airfoil extends from 0.5 to 1.0. Similarly, in low-speed flight, the winglet should not stall before the wing. For this case, although the wing reaches a maximum lift coefficient of 1.4, the winglet only needs to achieve about 1.2.

The relationship between the winglet lift coefficient and that of the main wing is unique for every

wing/winglet combination, and ideally, every combination would have a specifically designed winglet airfoil. In addition, the information needed to guide the airfoil design depends on the details of the winglet geometry, which in turn, are driven by the aerodynamic characteristics of the airfoil. Thus, the winglet/airfoil design process is iterative. Nevertheless, given the similarity of the current generation of competition sailplanes, the small performance benefit that would result does not warrant such an effort for each design. For this reason, the results presented in Fig. 1 are actually a composite of a number of individual design studies. Consequently, a small compromise in performance is made to obtain an airfoil that satisfies requirements for a wide range of low-speed winglet applications.

In addition to achieving the required lift-coefficient range, the winglet airfoil must operate over a particular range of Reynolds numbers. This is difficult because not only do the small chords of the winglet make these Reynolds numbers quite low, but also because of the wide range of Reynolds numbers over which the winglet airfoil must operate efficiently. As shown in Fig. 2, the tip chord of a winglet near stall speed corresponds to a Reynolds number of only 7.2×10^4 , while the root at high speeds operates at a Reynolds number as high as 1.0×10^6 . In designing an airfoil that must operate at such low Reynolds numbers, laminar separation bubbles and the associated increases in profile drag are important concerns.

Using the information presented in Figs. 1 and 2, the critical points of the airfoil design effort can be identified. As summarized in Fig. 3, the winglet airfoil must have a $c_{l,max} = 1.2$ over a Reynolds number range of 7.2×10^4 (tip) to 2.8×10^5 (root). The lower limit of the low-drag range is at $c_l = 0.5$, and this must be achieved for Reynolds numbers from 2.5×10^5 (tip) to 1.0×10^6 (root). The upper limit of the low-drag range is at $c_l = 1.0$, and must be achieved from $R = 8.4 \times 10^4$ (tip) to $R = 3.2 \times 10^5$ (root). It should be noted that low drag coefficients at the lowest Reynolds numbers are difficult to achieve. This is not of much concern, however, as the low Reynolds numbers are a consequence of the winglet planform tapering rapidly toward the tip. Even though the drag coefficients are likely to be large in that region, the amount of area affected is small and the actual contribution to drag will not be large.

Finally, unlike an airfoil designed for a wing, for this application, the pitching moment is not a design issue.

Design Procedure

An airfoil was designed to satisfy the set of requirements using the Eppler Airfoil Design and Analysis Code (PROFIL98).^{4,5} The result of this design effort is the PSU 94-097 airfoil. The first two digits in the designation indicate the year the airfoil was designed, 1994, and the last three are the thickness ratio in percent of chord, 9.7 percent. The shape of this airfoil and representative pressure distributions are shown in Fig. 4. The predicted section characteristics are presented in Fig. 5, and the airfoil coordinates in Table 1.

As shown in Fig. 5, although the desired lower lift-coefficient limit of the low-drag range was specified to be 0.5, the actual design effort uses a value that is 0.2 lower. This difference is intended as a margin for any uncertainties in the design specifications and the procedures, as well as to help manage tolerances in the manufacturing process. A similar margin is used at the upper lift-coefficient limit of the low-drag range.

The rapid drag increases that define the low-drag range, as can be observed in Fig. 5, are due to the boundary-layer transition point moving quickly toward the leading edge for lift coefficients greater than about 1.0 on the upper surface, and for lift coefficients less than about 0.3 on the lower surface. Thus, the lower lift-coefficient limit depends on the boundary-layer development on the lower surface at that point, which, in turn, depends on the lower surface pressure distribution. The design pressure distribution for this point is that presented in Fig. 4 for $\alpha = 2.0^\circ$. At this angle of attack, the pressure distribution has a nearly neutral gradient over much of the lower surface. This distribution is sufficient to maintain transition aft of the 50-percent chord location over most of the operational Reynolds number range. As the Reynolds number increases, the transition location gradually moves forward due to the boundary layer becoming less stable. For angles of attack less than 2.0° , transition is predicted to move quickly forward on the lower surface. This rapid movement is responsible for the sharp corner at the lower limit of the low-drag range that is depicted in Fig. 5. From this figure, it can be seen that the airfoil achieves the design goals for this part of the polar at the appropriate Reynolds numbers.

The upper limit of the low-drag range depends on the upper-surface pressure distribution at the lift coefficient that corresponds to $\alpha = 5.0^\circ$, shown in Fig. 4. The pressure distribution is initially very adverse and then decreasingly so. This results in a gradual forward movement of transition until $c_l = 1.0$. As the lift coefficient increases further, transition moves rapidly forward. Again, it is seen from the section characteristics in Fig. 5 that the winglet airfoil achieves

the required lift coefficients in the appropriate Reynolds number range. The higher drag at lower Reynolds numbers in the middle of the low-drag range is not a factor because the airfoil does not operate at those conditions.

At the low operational Reynolds numbers of this airfoil, the proper management of laminar separation bubbles is essential to a successful design. This is accomplished on both surfaces through the use of transition (instability) ramps that cause transition to occur through shallow pressure rises such that the separation bubble is prevented from thickening to such an extent that it causes an excessive drag increase.⁴ The shallow adverse pressure gradients present over the entire mid-chord region of the lower surface throughout the low-drag range, as can be seen in Fig. 4, are essentially transition ramps. While transition ramps are typically much less extensive, the long ramps employed here are necessitated by the low Reynolds numbers at which this airfoil operates. On the upper surface, a curved transition ramp, also seen in Fig. 4, extends from about 45-percent chord to nearly 65-percent throughout the low-drag range.

The upper-surface pressure distribution near the maximum lift condition, presented in Fig. 4, is characterized by a high suction peak. From the section characteristics in Fig. 5, the predicted maximum lift coefficient satisfies the design requirements.

Experimental Procedure

To verify the design result, particularly with regard to the low Reynolds number range of operation, the PSU 94-097 airfoil was wind-tunnel tested at Penn State.⁶ Measurements were taken for the range of Reynolds numbers from 2.4×10^5 to 1.0×10^6 . Although the tip region of the winglet can operate at lower values, a Reynolds number of 2.4×10^5 was the lowest possible without making modifications to the wind-tunnel drive system or building another model having a smaller chord.

Wind Tunnel, Model, and Data Acquisition System

The Penn State University Low-Speed, Low-Turbulence Wind Tunnel is a closed-throat, single-return atmospheric facility. The test section is rectangular, 3.3 ft high \times 4.8 ft wide, with filleted corners. The maximum test section speed is 220 ft/s. Airfoil models are mounted vertically in the test section and attached to electronically actuated turntables that allow the angle of attack to be set. The turntables are flush with the floor and ceiling and rotate with the model. The axis of rotation corresponds to the quarter-chord of the model. The gaps between the model and the turntables are sealed.

The flow quality of the Penn State wind tunnel has been measured and is well documented.^{7,8} Briefly, at a velocity of 150 ft/s, the flow angularity is below $\pm 0.25^\circ$ everywhere in the test section. At this velocity, the mean velocity variation in the test section are below ± 0.2 percent, and the turbulence intensity is less than 0.045 percent.

The model used for the PSU 94-097 airfoil measurements has a 1.0-ft chord. The span is such that the model extends completely over the 3.3-ft height of the test section. The model is constructed with fiberglass skins formed in molds that were manufactured using a computer-numerically-controlled milling machine. The model coordinates were verified at the midspan using a coordinate measuring machine. The root-mean-square average contour error is less than 0.003 in. The model has 39 pressure orifices on the upper surface and 32 on the lower surface. Each orifice has a diameter of 0.016 in and is drilled perpendicular to the surface. The orifice locations are staggered in the spanwise direction to minimize the influence of an orifice on those downstream.

To obtain drag measurements, a Pitot-static pressure probe is mounted from the ceiling of the tunnel. A traversing mechanism incrementally positions the probe across the wake. It is automatically aligned with the local wake streamline as the angle of attack changes. For these tests, the probe was positioned vertically at the tunnel centerline with the nose of the probe located 0.3 chords downstream of the model trailing edge.

The basic wind-tunnel pressures are measured using piezoresistive pressure transducers. Measurements of the pressures on the model are made by an automatic pressure-scanning system. Data are obtained and recorded using an electronic data-acquisition system.

Experimental Methods

The surface pressures measured on the model are reduced to standard pressure coefficients and numerically integrated to obtain section normal- and chord-force coefficients, as well as the section pitching-moment coefficients about the quarter-chord point. Section profile-drag coefficients are computed from the wake total and static pressures using standard procedures.^{9, 10} Low-speed wind-tunnel boundary corrections are applied to the data.¹¹ A total-pressure-tube displacement correction, although quite small, is also applied.⁹

The uncertainty of a measured force coefficient depends on the operating conditions and generally increases with increasing angles of attack.¹² In the higher lift regions, for which the uncertainty is the greatest, the measured lift coefficients have an uncertainty of $\Delta c_l = \pm 0.005$. The uncertainty of the drag

coefficients in low-drag range, is $\Delta c_d = \pm 0.00005$, and as the angle of attack approaches stall, this increases to $\Delta c_d = \pm 0.00015$. The pitching moment coefficients have an uncertainty of $\Delta c_m = \pm 0.002$

In addition to making the quantitative measurements indicated, flow-visualization studies were performed using fluorescent oil.¹³ In addition to being used to determine the locations and lengths of laminar separation bubbles as they depend on angle of attack, as well as to identify turbulent separation regions, this method was used to verify the two-dimensionality of the tests.

Experimental Results

Wind-tunnel measurements on the PSU 94-097 airfoil were obtained at selected Reynolds numbers. In addition to measurements being made with transition free (unforced), tests were made to determine if any overall gains were possible using artificial turbulators to prevent the formation of laminar separation bubbles.

Pressure Distributions

Pressure distributions for the PSU 94-097 airfoil at the lower limit of the low-drag range, $\alpha = 2^\circ$, for several Reynolds numbers are presented in Fig. 6. A laminar separation bubble can be observed in the upper-surface pressure distributions. At the lowest Reynolds number tested, 2.4×10^5 , the laminar separation occurs at about 60-percent chord, and turbulent reattachment is at approximately 78-percent chord. As the Reynolds number increases, the length of the separation bubble decreases. No bubble occurs on the lower surface over the entire low-drag range.

At the angle of attack corresponding to the upper limit of the low-drag range, $\alpha = 5^\circ$, the pressure distributions presented in Fig. 7 were obtained. Because the adverse pressure gradient is stronger than it is at $\alpha = 2^\circ$, the upper-surface laminar separation bubble at $R = 2.4 \times 10^5$ is about 10-percent chord further forward and is somewhat shorter than it is in that case. As the Reynolds number increases and the boundary layer becomes less stable, natural transition occurs before laminar separation and the bubble disappears.

Pressure distributions for $\alpha = 8^\circ$ at selected Reynolds numbers are presented in Fig. 8. At this angle of attack, except for a small increase in the leading-edge pressure peak with increasing Reynolds number, the distributions show little influence of Reynolds number. As confirmed by flow-visualization, a laminar separation bubble can be seen in the upper-surface pressure distributions. For $R = 2.4 \times 10^5$, this bubble extends from about 15-percent chord to 28-percent chord. Although it becomes shorter with increasing Reynolds numbers, it is present for all of the Reynolds

numbers of these tests. With increasing angles of attack, the bubble moves forward and decreases in length, persisting through stall to angles of attack beyond 18° .

Section Characteristics

The section characteristics of the PSU 94-097 airfoil for all Reynolds numbers tested are shown in Fig. 9. The airfoil maximum lift coefficient of 1.37 occurs for a Reynolds number of 1.0×10^6 at an angle of attack of 11° . When employed on a sailplane winglet, however, the airfoil would never operate simultaneously at high lift and high Reynolds number. As is typical, the value of the maximum lift coefficient decreases with decreasing Reynolds numbers. Nevertheless, in the range of Reynolds numbers at which the winglet must generate maximum lift, the $c_{l,max}$ of 1.29 exceeds the design requirement.

The low-drag range of the airfoil is significantly affected by the Reynolds number. As can be seen in Fig. 9, although the values of the drag coefficients in the low-drag range always decrease with increasing Reynolds numbers, the width of the low-drag range becomes narrower. The lower limit at $R = 1.0 \times 10^6$ occurs at $c_l = 0.5$, as specified by the design requirements. Likewise, the upper limit, $c_l = 1.0$, is also achieved at the appropriate Reynolds numbers. By not generating a more extensive low-drag range than required, the values of the drag coefficients are as low as they can be and still have the airfoil satisfy the given design requirements.⁴

In some airfoil measurements at low Reynolds numbers, a large variation of drag coefficient with spanwise station has been reported.¹⁴⁻¹⁶ This was explored during these tests, but no such variation was observed.

Section Characteristics with Turbulator Tape

The performance on airfoils operating at low Reynolds numbers can sometimes be improved by using some type of artificial turbulator to force the flow to transition before laminar separation occurs.¹⁷ By so doing, the drag due to the laminar separation bubble is eliminated. For an overall benefit, however, the drag reduction from eliminating the bubble must be greater than the drag due to the earlier transition plus that of the turbulator itself. To minimize the drag penalty due to the turbulator itself, it is important that it be no higher than the critical roughness height, the height sufficient to cause boundary-layer transition but not greater.¹⁸ The difficulty with the proper turbulator sizing for a winglet airfoil is due to the wide range of angles of attack and Reynolds numbers over which every spanwise station must operate. Using transition ramps intended to yield

thin separation bubbles that do not result in a significant drag penalty, the PSU 94-097 airfoil was designed to not benefit from the use of artificial turbulators. To determine if this effort was successful, measurements were made at a number of Reynolds numbers with zig-zag turbulators^{1, 17} of different thicknesses placed at the 50-percent chord location, just upstream of the laminar separation point for the upper limit of the low-drag range. It was found that a turbulator sized for $R = 2.4 \times 10^5$, a thickness of 0.016 in, reduces the drag slightly at that Reynolds number, results in essentially the same drag as the clean airfoil at $R = 3.0 \times 10^5$, and causes a progressively greater drag penalty as the Reynolds number increases. Although lower Reynolds numbers could not be tested, it is predicted that a thicker turbulator would be required to cause transition at Reynolds numbers of less than 2.0×10^5 .

From these results, the difficulty in employing a turbulator to reduce the drag is clear. If the turbulator is sized for the critical roughness height corresponding to high lift coefficients and low Reynolds numbers, then it is much too high and causes a significant drag penalty at lower lift coefficients and higher Reynolds numbers. If turbulator tape is only applied to those portions of the winglet that always operate at a low enough Reynolds number to benefit, then only the last few inches of the outboard portion of the winglet would be affected. It is questionable if such a small drag reduction over such a small area justifies the effort. This conclusion is supported by three-dimensional wind-tunnel measurements performed on an entire winglet that used the PSU 94-097 airfoil.¹⁹ In these experiments, in which the drag polar of the winglet itself was measured, it was found that artificial turbulators did not improve the lift-to-drag ratio of the winglet.

Comparison of Theoretical and Experimental Results

To validate the computational tools used in the design process, the experimental measurements were compared to predictions made using two well-known codes, PROFIL⁵ and XFOIL.²⁰ Both codes use a panel method to predict the outer (potential) flow, and account for viscous effects using an integral boundary-layer approach. In PROFIL, transition is predicted using a relatively new method that accounts for the upstream instability history of the boundary-layer by integrating the margin between the actual properties of the boundary layer at a point, and the values those properties would have if the boundary layer were neutrally stable at that point.²¹ Transition is predicted when the integrated amount of boundary-layer “instability” reaches a certain level. This information is also used in an empirical method to calculate the drag

due to laminar separation bubbles. Transition prediction in XFOIL is accomplished using a simplified envelope procedure for the so-called e^n -method.

Pressure Distributions

The comparisons of theoretical and experimental pressure distributions for the PSU 94-097 airfoil are presented in Fig. 10. The angles of attack of the experimental pressure distributions presented are for the design points, 2.0°, 5.0°, and 8.0°. They were measured at a Reynolds number of 1.0×10^6 . The inviscid theoretical results were calculated using PROFIL, and correspond to the same lift coefficients as the experimental ones. The agreement between the predicted and experimental pressure distributions is quite good except, of course, where laminar separation bubbles are present. The inviscid predictions do not account for laminar separation bubbles.^{4, 5} Because separation is not taken into account by the inviscid theory, the agreement between the predicted and measured pressure distributions deteriorates as the angle of attack increases.

Section Characteristics

The comparison of the theoretical and experimental section characteristics for a Reynolds number of 2.4×10^5 is presented in Fig. 11. The lift-curve slope is well predicted by XFOIL and appears to have been done so by PROFIL. In actuality, PROFIL simply uses a value of 2π /radian until separation is predicted at higher angles of attack. Once this occurs, a correction is applied to lift-curve slope, although it is apparent that this correction is not sufficient to fully account for the influence of the separated flow. The zero-lift angles of attack from both theories and the experiment are also in excellent agreement.

The prediction of $c_{l,max}$ by both methods is good. The PROFIL code achieves an accurate prediction of $c_{l,max}$ for airfoils having a rapid forward movement of the separation point with increasing angles of attack, but this is not the case if the forward movement is more gradual. For these cases, an empirical criterion has been developed that has given reasonably reliable results. Specifically, this criterion is that $c_{l,max}$ occurs when the upper-surface profile drag coefficient reaches the value given by

$$c_{d,u} = 0.0172 \times (1 \times 10^6 / R)^{1/8}$$

For this airfoil, this yields a $c_{l,max}$ that is in good agreement with the measured value. The XFOIL prediction, although slightly higher, is also close to the value measured.

Although the pitching-moment coefficient is not much of an issue for this airfoil, its prediction by PROFIL is somewhat too negative. The pitching-moment coefficient prediction by XFOIL is reasonably good.

The drag coefficients predicted by the two methods are in close agreement, and both agree well with the experimental results. Outside the low-drag range, the values from both theoretical methods and the measurements are essentially the same. The upper limit of the low-drag range is predicted slightly better by the PROFIL code, while the lower limit is predicted better by XFOIL. In the low drag range, the PROFIL predictions are somewhat closer to the measurements in the upper part of the range, and the experimental results are in between the two predictions in the lower part. Overall, given the problems of predicting and measuring aerodynamic characteristics at such low Reynolds numbers, the agreement among the two theories and the experiment is notable.

The theoretical predictions from the two methods are presented along with wind-tunnel results for $R = 4.0 \times 10^5$ in Fig. 12, and for $R = 1.0 \times 10^6$ in Fig. 13. For the most part the agreement becomes better as the Reynolds number increases. At $R = 1.0 \times 10^6$, the smooth forward movement of transition has caused the sharp corners of the low-drag range to disappear, and the predictions of the two theories and the experimental data are closer than at the lower Reynolds numbers. Still, the higher lift-coefficient region of the measured low-drag range is predicted more closely by PROFIL, while the lower lift-coefficient region is predicted more closely by XFOIL. In addition, the $c_{l,max}$ predictions of both methods are now slightly high, but still quite reasonable.

Concluding Remarks

An airfoil, the PSU 94-097, has been designed for use on winglets of high-performance sailplanes. Because of the low operational Reynolds number of this airfoil, along with the fact that it must operate well over such a wide range of Reynolds numbers, it is likely that improved winglet performance could be achieved by using different airfoils over the winglet span. In this way, the compromises necessary to accomplish the design requirements over such a broad operating range could be reduced, and the use of a family of airfoils, each designed to operate over a much narrower range of conditions, would benefit performance.

To validate the design effort, the PSU 94-097 airfoil was tested in the Penn State Low-Speed, Low-Turbulence Wind Tunnel. The section characteristics were also evaluated using two highly regarded two-dimensional airfoil codes. Overall, the agreement

between the theoretical predictions and the measurements is excellent. The good agreement between the two theories and, in turn, the agreement with the measurements, lends confidence to the theoretical design tools, and to the predicted airfoil performance itself. In all respects, the PSU 94-097 airfoil was found to satisfy the design requirements.

References

¹Thomas F., *Fundamentals of Sailplane Design*, Judah Milgram, translator and contributor, College Park Press, College Park, Maryland, 1999.

²Maughmer, M.D., "The Design of Winglets for High-Performance Sailplanes," AIAA Paper 2001-2406, June 2001.

³Maughmer, M.D. and Kunz, P.J., "Sailplane Winglet Design," *Technical Soaring*, Vol. 22, No. 4, Oct. 1998, pp. 116-123.

⁴Eppler, R., *Airfoil Design and Data*, Springer-Verlag, Berlin, 1990.

⁵Eppler, R., "Airfoil Program System: PROFIL98," User's Guide, Richard Eppler, Stuttgart, c.1998.

⁶Swan, T.S., "Low Reynolds Number Wind Tunnel Investigation of the PSU 94-097 Winglet Airfoil," M.S. Thesis, Dept. of Aerospace Engineering, Penn State Univ., University Park, PA, 2000.

⁷Brophy, C.M., "Turbulence Management and Flow Qualification of The Pennsylvania State University Low Turbulence, Low Speed, Closed Circuit Wind Tunnel," M.S. Thesis, Dept. of Aerospace Engineering, Penn State Univ., University Park, PA, 1993.

⁸Medina, R., "Validation of The Pennsylvania State University Low-Speed, Low-Turbulence Wind Tunnel Using Measurements of the S805 Airfoil," M.S. Thesis, Dept. of Aerospace Engineering, Penn State Univ., University Park, PA, 1994.

⁹Prankhurst, R.C. and Holder, D.W., *Wind-Tunnel Technique*, Sir Isaac Pitman & Sons, Ltd., London, 1965.

¹⁰Schlichting, H., "Determination of Profile Drag," Chapter XXV, *Boundary Layer Theory*, Seventh Edition, McGraw-Hill, New York, 1979, pp.758-779.

¹¹Allen, H.J. and Vincenti, W.G., "Wall Interference in a Two-Dimensional-Flow Wind Tunnel, With

Consideration of the Effect of Compressibility," NACA Report 782, 1944.

¹²Kline, S.J. and McClintock, F.A., "Describing Uncertainties in Single-Sample Experiments," *Mechanical Engineering*, Vol. 75, No. 1, Jan. 1953.

¹³Loving, D.L. and Katzoff, S., "The Fluorescent-Oil Film Method and Other Techniques for Boundary-Layer Flow Visualization," NASA MEMO 3-17-59L, 1959.

¹⁴Althaus, D., "Drag Measurements on Airfoils," *Technical Soaring*, Vol. VII, No. 1, Sept. 1981, pp. 9-12.

¹⁵Gulliemo, J.J. and Selig, M.S., "Spanwise Variations in Profile Drag Measurements for Airfoils at Low Reynolds Numbers," *Journal of Aircraft*, Vol. 33, No. 4, Aug. 1996, pp. 699-707.

¹⁶McGhee, R.J., Walker, B.S., and Millard, B.F., "Experimental Results for the Eppler 387 Airfoil at Low Reynolds Numbers in the Langley Low-Turbulence Pressure Tunnel," NASA Technical Memorandum 4062, Oct. 1988.

¹⁷Boermans, L.M.M., Donker Duyvis, F.J., van Ingen, J.L., and Timmer, W.A., "Experimental Aerodynamic Characteristics of the Airfoils LA 5055 and DU 86-084/18 at Low Reynolds Numbers," *Low Reynolds Number Aerodynamics*, T. J. Mueller (Editor), Lecture Notes in Engineering 54, Springer-Verlag, Berlin, 1989, pp. 115-13.

¹⁸Braslow, A.L. and Knox, E.C., "Simplified Method for Determination of Critical Height of Distributed Roughness Particles for Boundary-Layer Transition at Mach Numbers From 0 to 5," NACA TN 4363, 1958.

¹⁹Thorsen, O.R., "Theoretical and Experimental Analysis of the Winglet Designed for the High Performance Sailplane ASW-27," Low-Speed Aerodynamics Laboratory, Delft University of Technology, March 1999.

²⁰Drela, M., "XFOIL Documentation," User's Guide, Mark Drela, Cambridge, MA, c. 1989.

²¹Eppler, R., "An Empirical Criterion for Laminar-to-Turbulent Boundary-Layer Transition," *Technical Soaring*, Vol. 23, No. 2, April 1999, pp. 34-42.

Table 1 PSU 94-097 airfoil coordinates

UPPER SURFACE		LOWER SURFACE	
X	Y	X	Y
0.00008	0.00099	0.00000	0.00000
0.00164	0.00566	0.00002	-0.00044
0.00747	0.01362	0.00031	-0.00162
0.01749	0.02237	0.00109	-0.00264
0.03163	0.03144	0.00237	-0.00363
0.04983	0.04046	0.00450	-0.00484
0.07200	0.04913	0.01504	-0.00843
0.09803	0.05723	0.03099	-0.01135
0.12778	0.06457	0.05223	-0.01344
0.16104	0.07103	0.07861	-0.01473
0.19757	0.07655	0.10991	-0.01527
0.23701	0.08108	0.14580	-0.01515
0.27899	0.08456	0.18595	-0.01443
0.32305	0.08696	0.22994	-0.01325
0.36876	0.08819	0.27724	-0.01174
0.41564	0.08819	0.32729	-0.00998
0.46324	0.08687	0.37951	-0.00805
0.51121	0.08417	0.43325	-0.00602
0.55916	0.08011	0.48785	-0.00394
0.60678	0.07468	0.54273	-0.00177
0.65387	0.06808	0.59735	0.00039
0.70009	0.06072	0.65110	0.00238
0.74490	0.05297	0.70331	0.00407
0.78772	0.04510	0.75332	0.00535
0.82800	0.03739	0.80042	0.00612
0.86517	0.03004	0.84394	0.00635
0.89868	0.02324	0.88321	0.00603
0.92886	0.01720	0.91760	0.00522
0.95406	0.01223	0.94656	0.00405
0.97398	0.00834	0.96959	0.00270
0.98838	0.00554	0.98635	0.00141
0.99709	0.00385	0.99656	0.00041
1.00000	0.00328	1.00000	0.00000

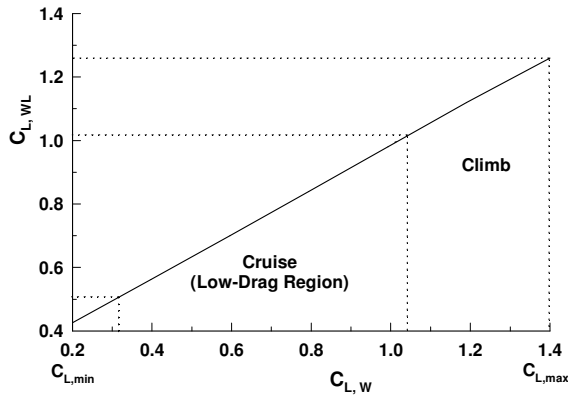


Fig. 1 Winglet lift-coefficient operating range compared to that of the wing for a typical high-performance sailplane.

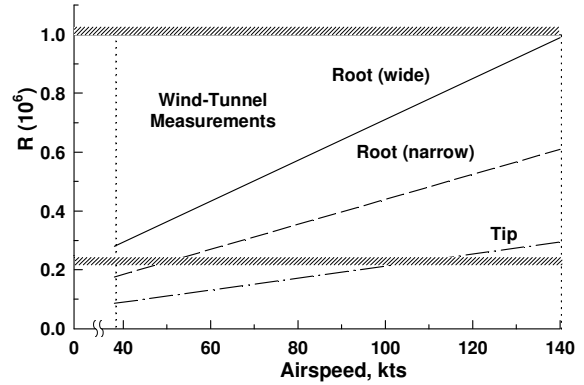


Fig. 2 Operational Reynolds number range of winglet airfoil and range of wind-tunnel tests.

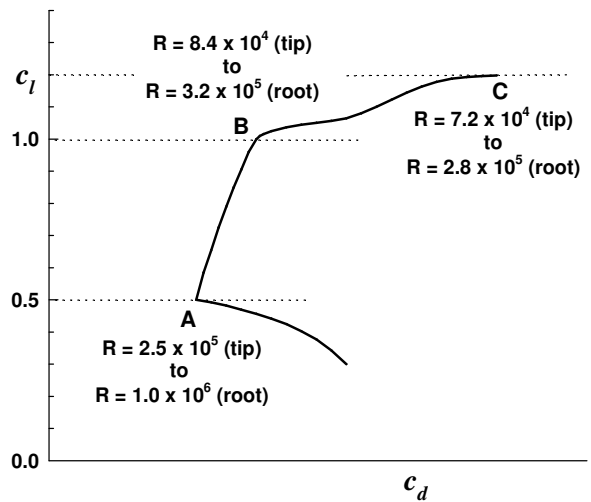


Fig. 3 Summary of design requirements for airfoil.

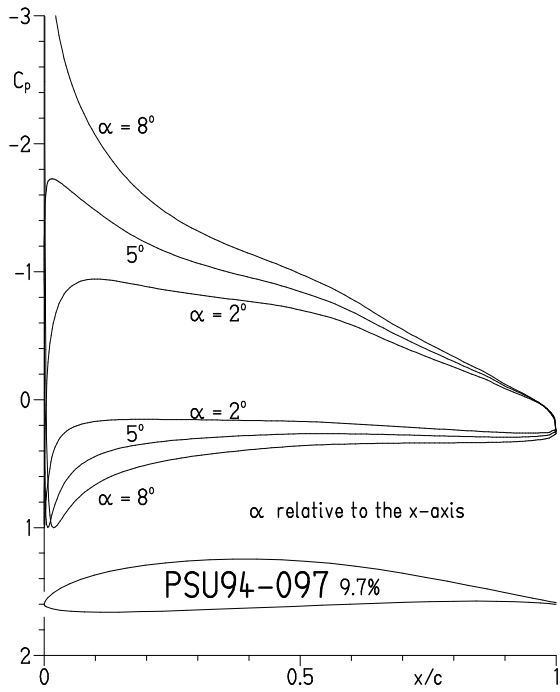


Fig. 4 The PSU 94-097 airfoil shape and inviscid velocity distributions.

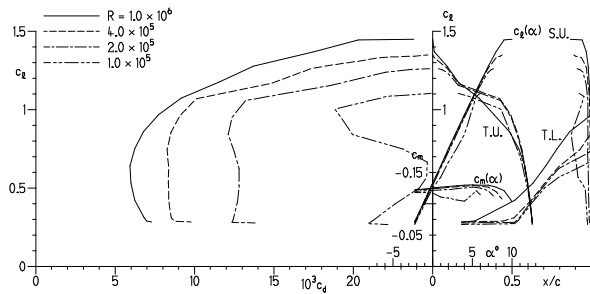


Fig. 5 Theoretical section characteristics of the PSU 94-097 airfoil, PROFIL98.

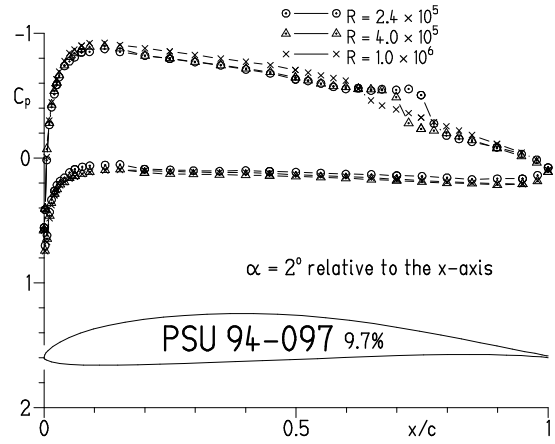


Fig. 6 Measured pressure distributions at $\alpha = 2^\circ$ and selected Reynolds numbers.

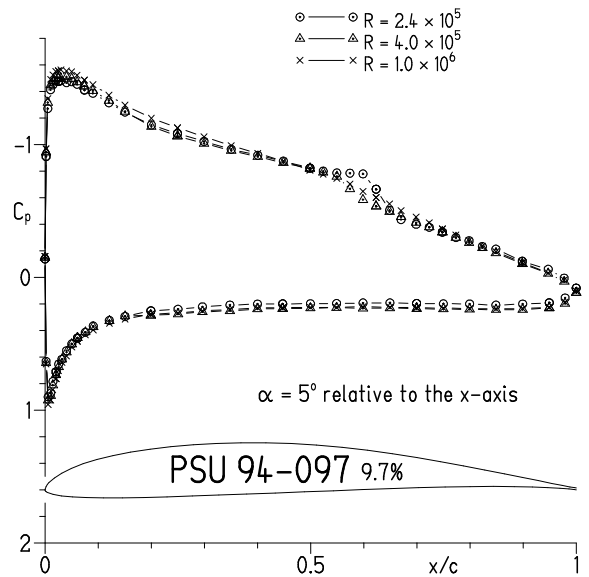


Fig. 7 Measured pressure distributions at $\alpha = 5^\circ$ and selected Reynolds numbers.

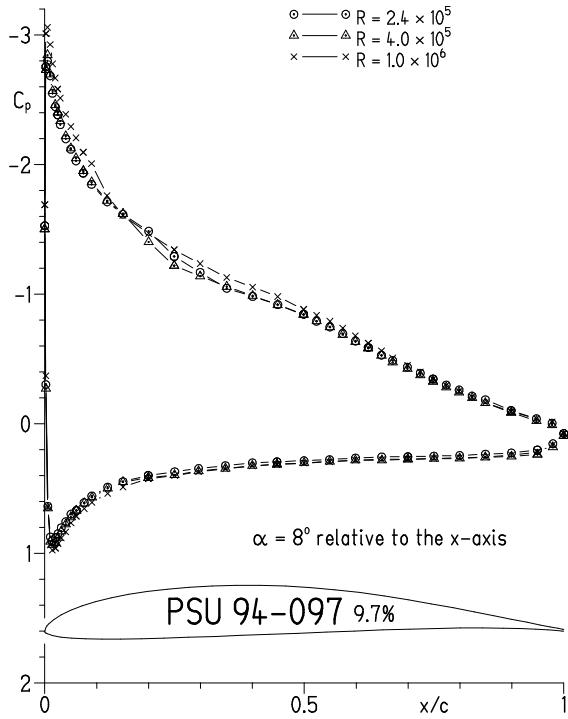


Fig. 8 Measured pressure distributions at $\alpha = 8^\circ$ and selected Reynolds numbers.

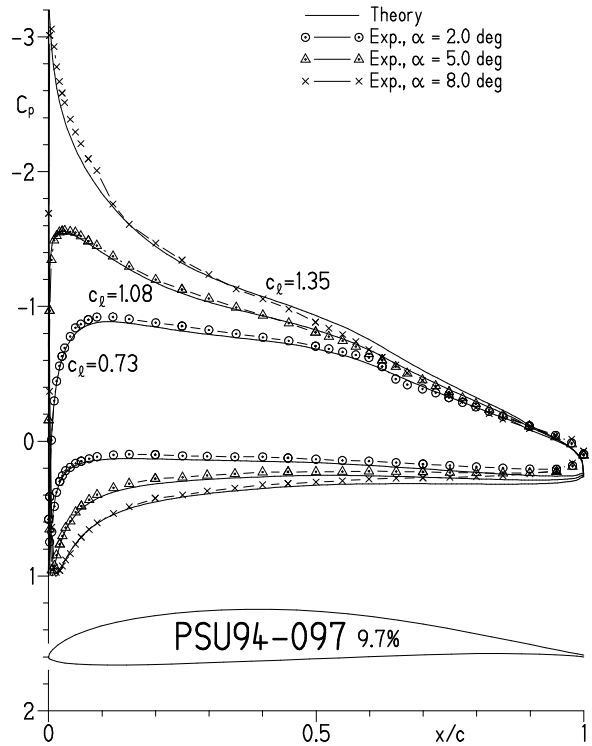


Fig. 10 Comparison of measured design point pressure distributions at $R = 1.0 \times 10^6$ to inviscid theory.

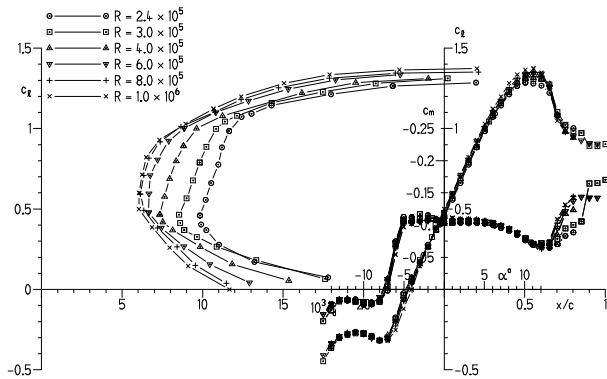


Fig. 9 Measured section characteristics of the PSU 94-097 airfoil.

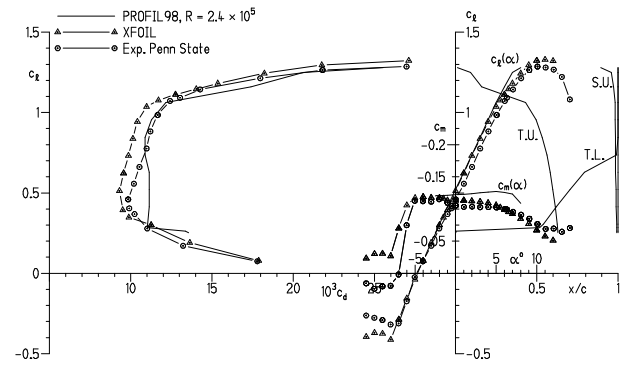


Fig. 11 Comparison of theoretical and experimental section characteristics for $R = 2.4 \times 10^5$.

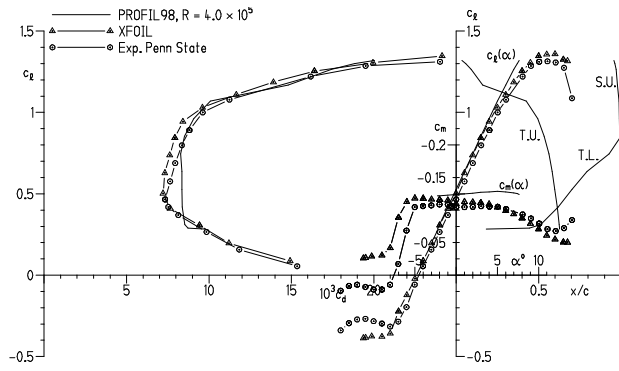


Fig. 12 Comparison of theoretical and experimental section characteristics for $R = 4.0 \times 10^5$.

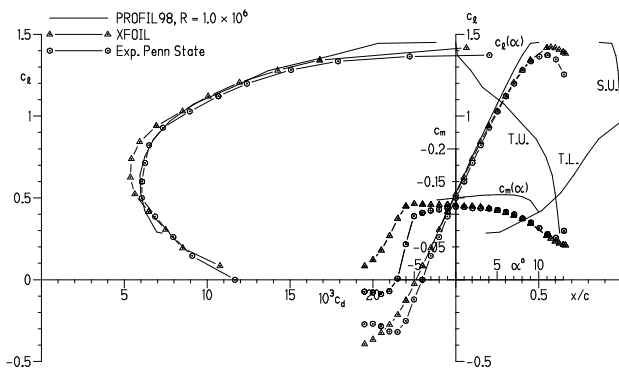


Fig. 13 Comparison of theoretical and experimental section characteristics for $R = 1.0 \times 10^6$.